HHS Public Access

Author manuscript

Adv Exp Med Biol. Author manuscript; available in PMC 2017 January 05.

Published in final edited form as:

Adv Exp Med Biol. 2016 ; 923: 43–50. doi:10.1007/978-3-319-38810-6_6.

Chapter 6: Magnification of Cholesterol-Induced Membrane Resistance on the Tissue Level: Implications for Hypoxia

Ryan Shea,

Department of Chemistry, New Mexico Institute of Mining and Technology (New Mexico Tech), 801 Leroy Place, Socorro, NM 87801, USA. Department of Mathematics, Chemistry, and Physics, West Texas A&M University, Canyon, TX, USA

Casey Smith, and

Department of Chemistry, New Mexico Institute of Mining and Technology (New Mexico Tech), 801 Leroy Place, Socorro, NM 87801, USA

Sally C. Pias

Department of Chemistry, New Mexico Institute of Mining and Technology (New Mexico Tech), 801 Leroy Place, Socorro, NM 87801, USA

Abstract

High cellular membrane cholesterol is known to generate membrane resistance and reduce oxygen (O_2) permeability. As such, cholesterol may contribute to the Warburg effect in tumor cells by stimulating intracellular hypoxia that cannot be detected from extracellular oxygen measurements. We probe the tissue- level impact of the phenomenon, asking whether layering of cells can magnify the influence of cholesterol, to modulate hypoxia in relation to capillary proximity. Using molecular dynamics simulations, we affirm that minimally hydrated, adjacent lipid bilayers have independent physical behavior. Combining this insight with published experimental data, we predict linearly increasing impact of membrane cholesterol on oxygen flux across cells layered in tissue.

Keywords

Cholesterol; Cancer; Molecular dynamics simulation; Oxygen bioavailability; Kinetics

1 Introduction

Here, we consider intracellular oxygen bioavailability and the potential impact of membrane resistance as a hindrance to oxygen flux. In particular, we examine the kinetics of oxygen transport across a series of several membranes, relevant to cells buried between capillaries, especially within tumors.

Several investigations provide valuable evidence that oxygen flux is reduced by substantial membrane cholesterol incorporation. Swartz and colleagues [1] demonstrated, using electron paramagnetic resonance (EPR) oximetry, that cultured mammalian cell lines with distinct membrane cholesterol levels differ in intracellular oxygenation. Using a technique that differentiates intra- and extracellular oxygen measurements, the group showed that an

oxygen gradient could be observed across the plasma membrane. Assays were performed on three Chinese hamster ovary (CHO) cell lines with phenotypic differences in cholesterol metabolism and plasma membrane cholesterol level. The magnitude of the oxygen gradient increased with the plasma membrane cholesterol concentration. Manipulation of the cholesterol level in the cell lines, likewise, influenced the gradient, with increasing cholesterol content tending to decrease intracellular oxygenation relative to extracellular [1].

Such a gradient could arise if the rate of oxygen consumption exceeded the rate of replenishment. Thus, the work suggests that high-cholesterol plasma membranes can present a measureable barrier to oxygen transport. We especially note from the CHO cell study that plasma membrane cholesterol content can influence intra-cellular oxygenation in a manner not directly interpretable from extracellular measurements.

The view of high-cholesterol cell membranes as a barrier is further affirmed in studies of red blood cell (RBC) oxygenation by Buchwald and colleagues [2, 3]. Specifically, the rate of oxygen uptake and release declines with the plasma membrane cholesterol content of RBCs [3]. As a result, RBC oxygen saturation is diminished, and oxygen release upon demand is diminished [2]. The authors propose that angina pectoris in patients with hypercholesterolemia may be caused partly by reduced oxygen release from RBCs with elevated membrane cholesterol, contributing to heart muscle hypoxia and painful lactic acid buildup [3].

These studies, together, present compelling evidence that high-cholesterol membranes present a *kinetic* barrier to oxygen transport. Biophysical experiments with EPR oximetry reinforce this view. Subczynski and colleagues have found that cholesterol reduces the membrane oxygen permeability coefficient (a descriptor of flux) by several-fold, compared with phospholipid alone [4, 5]. Given this resistance to oxygen transport, Brown and Galea previously suggested that cholesterol may contribute to the Warburg effect in cancer cells [6]. Indeed, the existing evidence strongly implies that intracellular hypoxia is possible, even when extracellular oxygen is abundant.

We investigate the tissue-level impact of reduced oxygen flux through cholesterol- rich membranes. We do so by examining the structural and functional independence of bilayers placed very close together, representing direct juxtaposition of plasma membrane segments in layered cells. We combine the results with experimentally derived flux information to predict how plasma membrane cholesterol impacts oxygen bioavailability within tissue, given the necessity of crossing multiple membranes to reach mitochondria in cells buried between capillaries.

2 Methods

We have used all-atom molecular dynamics simulations of two adjacent bilayers separated by a thin water layer to calculate electron density and oxygen diffusional free energy profiles. All simulations used the GPU/CUDA-accelerated implementation [7] of the Amber 14 or Amber 12 biomolecular simulation software [8, 9], along with the Lipid14 force field [10] and a cholesterol extension by Ross Walker and Benjamin Madej [11]. We developed

O_2 parameters in our laboratory, defining the bond length as 1.21 Å from the CRC Handbook [12], with a vibrational force constant of 849.16 kcal/mol • $Å^2$ based on Raman spectroscopic measurements [13] and with all other parameters defined the same as the carbonyl oxygen (oC) atom type in Lipid11 [14].

Lipid bilayers were constructed initially using the CHARMM-GUI membrane builder [15, 16]. A bilayer containing 1-palmitoyl-2-oleoylphosphatidylcholine (POPC) and cholesterol in a 1:1 ratio was built with 128 lipids total, including 32 POPC and 32 cholesterol molecules per leaflet and was pre-equilibrated for 500 ns using the GAFFLipid force field [17] with the Lipid11 cholesterol parameters [14]. The Lipid14 force field [10] with a cholesterol extension by Ross Walker and Benjamin Madej [11] was used throughout the remaining simulations. The pre- equilibrated POPC/cholesterol system was further equilibrated for 200 ns with this force-field combination. Its closest 15 water molecules per lipid molecule (“per lipid”) were retained using the AmberTools [8] program CPPTRAJ [18], and this minimally hydrated POPC/cholesterol structure was used as the starting configuration for “double bilayer” simulations.

All simulations used the TIP3P water model [19]. Through trial-and-error, we established that bilayers separated by 15 waters per lipid remained structurally distinct, while bilayers separated by only 10 waters per lipid showed physical fusion behavior early in the simulations.

Bonds to hydrogen were constrained using the SHAKE algorithm [20], allowing a 2-fs timestep. A constant temperature of 310 K (37 °C) was maintained using Langevin dynamics with a collision frequency of 1 ps^{-1} during the equilibration phases and using the Berendsen thermostat [21] during the production phase. A constant pressure of 1 atm was maintained using the Berendsen barostat [21] during the pre-equilibration and the Monte Carlo barostat (as implemented in Amber 14) thereafter.

A POPC bilayer was constructed with CHARMM-GUI, including 15 waters per lipid. This bilayer was size-matched with the pre-equilibrated POPC/cholesterol structure described above, based on an expected POPC area per lipid calculated from previous simulations. This surface-area matching called for 82 POPC lipids, with 41 in each leaflet. We used PackMol [22] to place the POPC bilayer close to the pre-equilibrated POPC/cholesterol bilayer. This double bilayer system was minimized over 20,000 steps, heated from 100 to 310 K over 100 ps, then equilibrated for 200 ns prior to adding oxygen.

O_2 molecules were introduced by replacing water molecules between the bilayers, and the double bilayer systems with oxygen were minimized and heated in the same manner as above, while applying a Cartesian restraint on the O_2 molecules with a force constant of 5 kcal/mol • $Å^2$. An O_2 concentration of 200 mM was used for the entire molecular system (water and lipid). Though higher than the concentration of air-equilibrated water (approximately 200 μM), this concentration allows the O_2 molecules to diffuse independently while facilitating rapid sampling of the O_2 configurational space [see also 23]. Production simulations were run without restraints for 300 ns.

Free energy and electron density profiles were calculated using CPPTRAJ. The free energy was calculated at 1-Å intervals (bins) along the bilayer normal, z, following the approach of Marrink and Berendsen that applies the relationship $G(z) = -RT \ln\{C(z)/C_{max}\}$, where $C(z)$ is the O_2 population of a given z bin and C_{max} is the population of the most populated bin [24].

3 Results and Discussion

The constituent POPC and POPC/cholesterol bilayers in the minimally hydrated "double bilayer" system remain structurally independent. As such, the electron density and free energy profiles of both bilayers (Fig. 6.1) closely resemble those calculated in our laboratory for single bilayer systems (data not shown). This observation agrees with prior experimental work demonstrating that the structural distinctness of lipid bilayers is maintained by headgroup-associated hydration repulsion [reviewed in 25]. Thus, we treat each bilayer as having independent oxygen transport behavior in the analysis that follows.

Subczynski and colleagues found in EPR oximetry studies that incorporation of cholesterol in a 1:1 ratio with phospholipid results in a three- to five-fold reduction in the permeability coefficient for oxygen flux [4, 5]. Based on free energy barriers alone and not accounting for the diffusional/collisional behavior of oxygen, we predict a rate reduction of the same order of magnitude as the EPR study (data not shown). We recently have investigated the impact of higher cholesterol concentrations on oxygen transport and have found a consistent decrease in the predicted rate of oxygen transport with modest increases in cholesterol content (publication forthcoming).

Yet, what is the tissue-level impact of membrane resistance? To reach mitochondria, oxygen must diffuse across a minimum of two cholesterol-containing membranes—namely, the plasma membrane of the red blood cell and the plasma membrane of the target cell. Endothelial cell membranes may also intercede, presenting an additional barrier if the cholesterol content is substantial. For cells buried between capillaries, oxygen will then diffuse via the path of least resistance until it reaches its site of consumption. Assuming highly permeable cellular membranes, it seems likely that the most favorable path will normally involve passage from membrane to membrane [26, 27], as the membrane interior provides a low-energy environment for oxygen (observable in Fig. 6.1).

If oxygen were required to pass through several membranes, the rate of diffusion would be reduced in proportion to the number of resistant membranes. Supposing a series of equally resistant membranes, we predict the kinetic impact of passing oxygen across several cell layers. Figure 6.2 projects the cumulative effect on oxygen flux when several cholesterol-rich membranes are traversed, assuming a three- or five-fold reduction in permeability per membrane. The overall rate impact is expected to depend linearly on the number of membranes crossed and on the magnitude of resistance presented by each membrane. In the case that an individual membrane reduces oxygen permeability by three-fold, ten sequential membranes are anticipated to decrease oxygen flux by 30-fold, reaching 1/30 or roughly 3 % of the unhindered flux.

The above analysis describes a “worst-case scenario” for oxygen diffusion across cholesterol-rich tissues. In actual tissue, it is likely that oxygen may find alternative, lower-resistance paths for diffusion that avoid some of the large energy barriers presented by cholesterol-rich membranes. For example, oxygen may pass around cells through the extracellular space. Thus, the degree of overall flux reduction may be lower than predicted with our current model. Even if diffusion through extracellular space were possible, the diffusional path-length required for avoiding passage across resistant cells would increase relative to the membrane-to-membrane diffusion scenario, generating a reduction in flux proportional to the path-length. Further modeling that takes the possibility of diffusion through extracellular space into account may be informative.

It is also important to note that our model greatly simplifies the structure of biological membranes. We have examined membranes incorporating only POPC phospholipid and cholesterol, while actual membranes incorporate many other types of phospholipid, along with substantial amounts of protein. Membrane proteins, like cholesterol, may reduce the permeability of membrane lipids, and the proteins, themselves, may have very low oxygen permeability [4, 28, 29]. Further, we have assumed compositional homogeneity across the leaflets of the bilayer, while plasma membranes are known to differ in the lipid composition of the extra-cellular and intracellular leaflets. We plan to address such complexities of cellular membrane structure in future modeling work. Moreover, we intend to use our models in conjunction with oxygen measurements in living cells, under conditions predicted by the models to influence intracellular oxygenation.

4 Conclusion

The capacity of cholesterol-rich cellular membranes to hinder oxygen diffusion may result in intracellular hypoxia not discernable from extracellular measurements. Even modest reduction of flux across a single membrane could substantially impact tissue oxygenation, due to magnification of the rate effect when oxygen must traverse several membranes or navigate around intervening cells.

Acknowledgments

Financial support for this project was provided by the NM-INBRE program, which is funded by National Institutes of Health grant P20GM103451 through NIGMS. Further financial support was generously provided by the Glendorn Foundation. The project used computing resources of the Extreme Science and Engineering Discovery Environment (XSEDE), which is supported by National Science Foundation grant number ACI-1053575. We thank Snežna Rogelj for her ongoing inspiration and biological insight, Jeff Altig for helpful conversations, and Ryan Bredin for developing our O_2 force field parameters. We gratefully acknowledge Ross Walker and Benjamin Madej for providing advance access to their updated cholesterol force field parameters. Finally, we appreciate the thoughtful review of our manuscript by members of the International Society on Oxygen Transport to Tissue (ISOTT).

References

1. Khan N, Shen J, Chang TY, et al. Plasma membrane cholesterol: a possible barrier to intracellular oxygen in normal and mutant CHO cells defective in cholesterol metabolism. Biochemistry. 2003; 42(1):23–29. [PubMed: 12515536]
2. Steinbach JH, Blackshear PL, Varco RL, Buchwald H. High blood cholesterol reduces in vitro blood oxygen delivery. J Surg Res. 1974; 16(2):134–139. [PubMed: 4818338]

3. Menchaca HJ, Michalek VN, Rohde TD, et al. Decreased blood oxygen diffusion in hypercholesterolemia. Surgery. 1998; 124(4):692–698. [PubMed: 9780990]
4. Widomska J, Raguz M, Subczynski WK. Oxygen permeability of the lipid bilayer membrane made of calf lens lipids. Biochim Biophys Acta. 2007; 1768(10):2635–2645. [PubMed: 17662231]
5. Subczynski WK, Hyde JS, Kusumi A. Oxygen permeability of phosphatidylcholine-cholesterol membranes. Proc Natl Acad Sci. 1989; 86(12):4474–4478. [PubMed: 2543978]
6. Galea AM, Brown AJ. Special relationship between sterols and oxygen: were sterols an adaptation to aerobic life? Free Radic Biol Med. 2009; 47(6):880–889. [PubMed: 19559787]
7. Salomon-Ferrer R, Götz AW, Poole D, et al. Routine microsecond molecular dynamics simulations with AMBER on GPUs. 2. Explicit solvent particle mesh Ewald. J Chem Theory Comput. 2013; 9(9):3878–3888. [PubMed: 26592383]
8. Case, DA.; Berryman, JT.; Betz, RM., et al. AMBER 2015. University of California; San Francisco: 2015.
9. Case, DA.; Darden, TA.; Cheatham, TE., III, et al. AMBER 12. University of California; San Francisco: 2012.
10. Dickson CJ, Madej BD, Skjevik AA, et al. Lipid14: the Amber lipid force field. J Chem Theory Comput. 2014; 10(2):865–879. [PubMed: 24803855]
11. Madej B, Gould IR, Walker RC. A parameterization of cholesterol for mixed lipid bilayer simulation within the Amber Lipid14 force field. J Phys Chem B. 2015; 119(38):12424–12435. [PubMed: 26359797]
12. Weast, RC., editor. CRC Handbook of Chemistry and Physics. 67. The Chemical Rubber Co; Boca Raton: 1986.
13. Herzberg, G.; Spinks, JWT. Molecular Spectra and Molecular Structure: Diatomic Molecules. Vol. 1. van Nostrand; New York: 1950.
14. Skjevik AA, Madej BD, Walker RC, Teigen K. LIPID11: a modular framework for lipid simulations using Amber. J Phys Chem B. 2012; 116(36):11124–11136. [PubMed: 22916730]
15. Jo S, Kim T, Iyer VG, Im W. CHARMM-GUI: a web-based graphical user interface for CHARMM. J Comput Chem. 2008; 29(11):1859–1865. [PubMed: 18351591]
16. Jo S, Lim JB, Klauda JB, Im W. CHARMM-GUI membrane builder for mixed bilayers and its application to yeast membranes. Biophys J. 2009; 97(1):50–58. [PubMed: 19580743]
17. Dickson CJ, Rosso L, Betz RM, et al. GAFFlipid: a General Amber Force Field for the accurate molecular dynamics simulation of phospholipid. Soft Matter. 2012; 8(37):9617.
18. Roe DR, Cheatham TE. PTRAJ and CPPTRAJ: software for processing and analysis of molecular dynamics trajectory data. J Chem Theory Comput. 2013; 9(7):3084–3095. [PubMed: 26583988]
19. Jorgensen WL, Chandrasekhar J, Madura JD, et al. Comparison of simple potential functions for simulating liquid water. J Chem Phys. 1983; 79(2):926.
20. Ryckaert J-P, Ciccotti G, Berendsen HJ. Numerical integration of the Cartesian equations of motion of a system with constraints: molecular dynamics of n-alkanes. J Comput Phys. 1977; 23(3):327–341.
21. Berendsen HJC, Postma JPM, van Gunsteren WF, et al. Molecular dynamics with coupling to an external bath. J Chem Phys. 1984; 81(8):3684.
22. Martinez L, Andrade R, Birgin E, Martinez J. Packmol: a package for building initial configurations for molecular dynamics simulations. J Comput Chem. 2009; 30:2157–2164. [PubMed: 19229944]
23. Wang Y, Cohen J, Boron WF, et al. Exploring gas permeability of cellular membranes and membrane channels with molecular dynamics. J Struct Biol. 2007; 157(3):534–544. [PubMed: 17306562]
24. Marrink S-J, Berendsen HJC. Simulation of water transport through a lipid membrane. J Phys Chem. 1994; 98(15):4155–4168.
25. Schneck E, Sedlmeier F, Netz RR. Hydration repulsion between biomembranes results from an interplay of dehydration and depolarization. Proc Natl Acad Sci. 2012; 109(36):14405–14409. [PubMed: 22908241]

26. Dutta A, Popel AS. A theoretical analysis of intracellular oxygen diffusion. J Theor Biol. 1995; 176(4):433–445. [PubMed: 8551742]

27. Sidell BD. Intracellular oxygen diffusion: the roles of myoglobin and lipid at cold body temperature. J Exp Biol. 1998; 201(Pt 8):1119–1128. [PubMed: 9510524]

28. Ashikawa I, Yin JJ, Subczynski WK, et al. Molecular organization and dynamics in bacteriorhodopsin-rich reconstituted membranes: discrimination of lipid environments by the oxygen transport parameter using a pulse ESR spin-labeling technique. Biochemistry. 1994; 33(16):4947–4952. [PubMed: 8161556]

29. Kawasaki K, Yin JJ, Subczynski WK, et al. Pulse EPR detection of lipid exchange between protein-rich raft and bulk domains in the membrane: methodology development and its application to studies of influenza viral membrane. Biophys J. 2001; 80(2):738–748. [PubMed: 11159441]

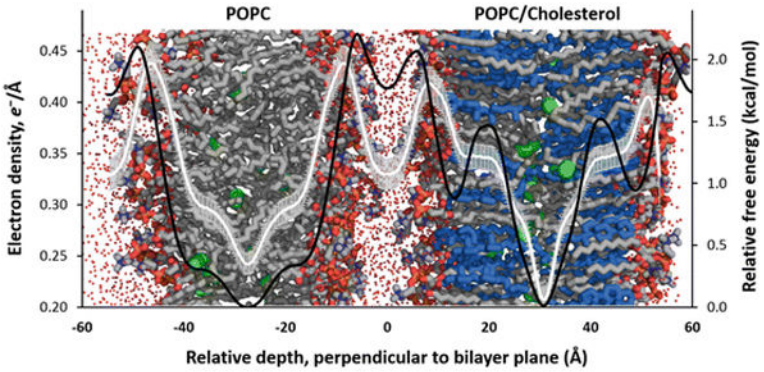

Fig. 6.1.

Electron density and free energy profiles are independent for hydrated bilayers in close proximity. The image shows a double bilayer system image overlaid with electron density (*white line*) and relative free energy (*black line*) plotted against relative depth perpendicular to the bilayer plane. The *left* bilayer contains only POPC, and the *right* contains POPC and cholesterol in a 1:1 ratio. The bars on the electron density *curve* indicate the standard deviation. Both curves were calculated from a single trajectory, covering 300 ns of production. The small *red points* indicate the positions of explicit water molecules, simplified for clarity. Bilayers: POPC carbon atoms—*gray*, cholesterol carbon atoms—*blue*, O_2 molecules—*green* spheres. All hydrogen atoms omitted for clarity

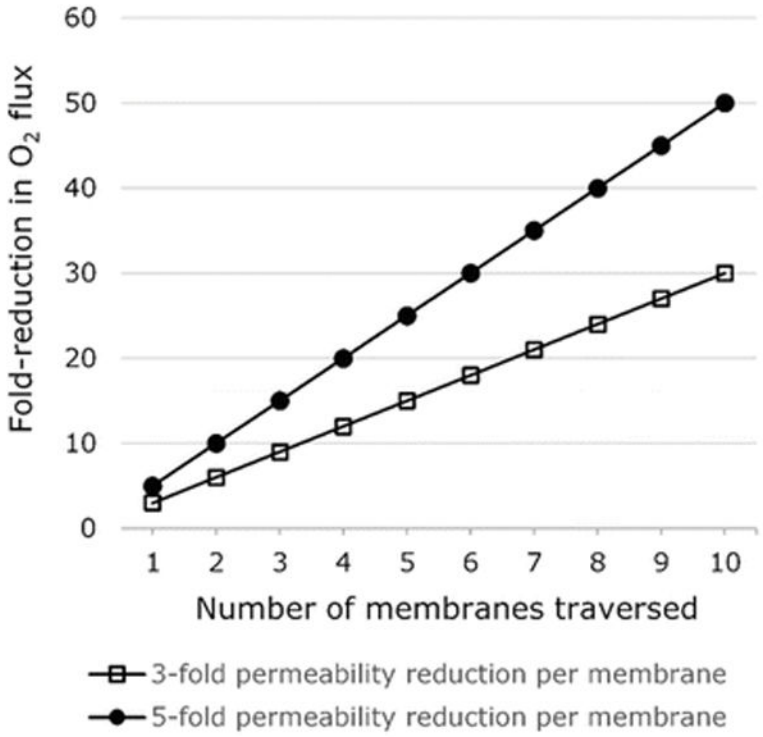

Fig. 6.2.
Predicted magnification of flux reduction as O_2 traverses multiple cell layers